Composites of transition metal-polyoxometalates with reduced graphene oxide as efficient bifunctional electrocatalysts for metal-air batteries

Filipe Machado Botelho de Gusmão

Instituto Superior Técnico, Universidade de Lisboa, 1049-001 Lisboa, Portugal

Abstract

This thesis analyses the potential of polyoxometalates (POMs) as alternatives to noble metal-based electrocatalysts, further considering their contribution to face the challenges of upgrading modern energy systems into more sustainable ones. As polyatomic ions with closed 3-dimensional frameworks, with many redox active sites, POMs have a specially interesting structure that could enable them to act as powerful electrocatalysts for electrochemical energy conversion and storage. They are cheaper and easier to obtain on a large scale than the noble metals electrocatalysts currently representing the most used ones in industrial electrochemical energy storage and conversion. After reviewing POMs current use in batteries, supercapacitors, fuel cells, and electrolysers, fundamental studies were carried out for five transition-metal based POMs containing manganese, iron, cobalt, nickel, and copper, all coordinated with reduced graphene oxide (rGO) to ascertain their viability as catalysts for the oxygen evolution reaction (OER), oxygen reduction reaction (ORR), and hydrogen evolution reaction (HER). For OER, the best material was found to be Ni-POM/rGO, for ORR it was Co-POM/rGO, and all of them were found not to be active for HER catalysis. Different POM:rGO ratios were also tested in order to optimise composition, and a ratio of 1:5 Ni-POM:rGO was found to be the most active for OER. Finally, metal-air batteries were built to optimise power density, again testing each POM to find out which is the most active. For the batteries, the best setup was using 4M KOH as electrolyte, and Co-POM/rGO as the catalyst.

Keywords: Polyoxometalates; Transition metals; Reduced Graphene Oxide; Metal-air batteries; Oxygen Evolution Reaction; Oxygen Reduction Reaction

1. Introduction

Climate change is already taking its toll. At the 77th session of the UN General Assembly (UNGA 77) held in New York City from 13 to 27 September 2022, after visiting Pakistan, where devastating floods threw nearly 1/3 of the country underwater, affecting 33 million people, the UN Secretary-General defended that climate action must be the first priority of every Government, and Global greenhouse gas emissions must be reduced in 45% by 2030 to allow reaching net zero by 2050.

Nonetheless, despite all evidence that action must be taken, greenhouse gas emissions are expected to increase around 14% this decade [1]. Developing and putting in place industrial energy storage and production options that do not emit greenhouse gases should be priorities for all developed countries.

Important breakthroughs have been made in the field of renewable energy production, which is a significant part of the solution to curb greenhouse emissions, with major investments already in place in many countries across Europe. But sustainable renewable energy production relies on efficient energy storage, as its production varies widely throughout the day and the year. Efficient energy storage guarantees that this energy becomes available in a way consistent with demand.

Using hydrogen as an energy carrier is a good option already in use. Even if most hydrogen currently comes from hydrocarbon reforming, a major source of greenhouse gas emissions, green hydrogen gas can be produced using electrolysis cells powered by renewable energy sources. Adding to this, hydrogen can be fed to fuel cells to generate electricity. However, scaling up this technology to industrial levels has proven to be difficult. As oxygen evolution reaction (OER) has slow kinetics, it requires high overpotentials for reasonable currents to develop, and the electrocatalysts typically used to reduce the electrical uptake of this reaction are made of high-cost and rare materials such as iridium and ruthenium. The best-performing low-cost catalysts normally operate in current ranges below 100 mA cm^{-2}, which are unsuitable for industrial use. The study of low-cost and high-performing catalyst materials is also difficult. Since it is usually conducted in small-scale lab cells, the conditions of temperature, pressure, and electrolyte concentration values are

bound to differ when scaling up to industrial cells, giving rise to significant divergences in electrolyte conductivity, ion migratory flux, and catalyst structural stability [2].

POMs, on the other hand, have shown high thermal stability, high sensitivity to electricity, and resistance to oxidative decomposition when used in catalysis, making them prime options for electrocatalytic study. Although POM-salts are mostly insulators, it is now possible to attach POMs to conductive and high-surface area materials through covalent or non-covalent means, using materials generated by nanostructured conductive carbons such as carbon nano-tubes (CNTs) and graphene [3]. “Wiring” of POMs to conductive organic polymers has also been suggested as a way to overcome the issue of their low conductivity [4]. It seems possible, then, to overcome POMs low conductivity, and produce reliable electrical connection between the POM as the reaction centre and other parts of the device, thus enabling the technological use of POMs in electrical devices.

POMs have exhibited the potential for multi-electron transfer, with their unique redox properties allowing the reversible uptake of up to 24 electrons per cluster unit (for example: $[PMo_{12}O_{40}]^{3-}$), which has been observed in the solid state [4-9]. Furthermore, their exact electrochemical properties such as redox potentials and number of stored electrons can be manipulated by chemical modification of the POM structure, one of the methods available being the incorporation of redox-active metal centres in them. Metal functionalization can also be used to generate coordinative substrate binding sites for electrochemical and electroanalytical applications [4]. Finally, there is already a large body of knowledge around these materials and applications in material and medical sciences are currently in place, supporting the potential scalability of these materials to industrial levels.

POMs have thus interesting properties for OER, ORR, and HER electrocatalysis, with potentially good activity, low cost, and scalability. This study aims at exploring the use of six transition-metal based POMs containing manganese, iron, cobalt, nickel, and copper as electrocatalysts for OER, ORR, HER electrocatalysis and as catalyst for metal/air batteries, while also addressing their potential to overcome the problems encountered with other materials in the search for efficient production and storage of green hydrogen in industry.

To that end, we first reviewed the existing research on these materials as electrocatalysts for the OER, ORR and HER reactions, and their use in batteries and supercapacitors. We then proceed to study five synthesized POM-transition metal hybrids. The synthesized POMs were characterized according to their structure, diffraction data, surface functionality, surface morphology and atomic composition. They were tested as catalysts for OER, HER, ORR and as a catalyst for metal-air batteries. We then discuss the results obtained, comparing their behaviour and cost with the most commonly used materials. We further conclude which one performs best.

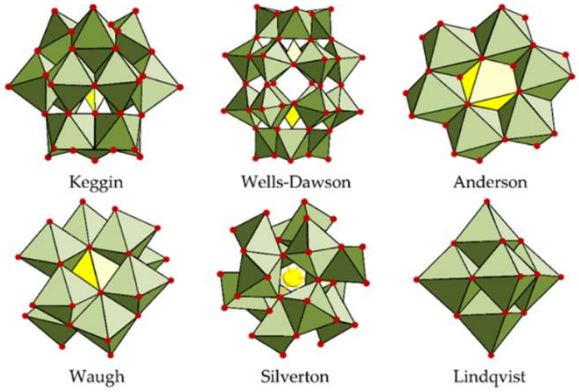

Figure 1. POM structures in polyhedral representations [10].

2. Fundamental electrocatalytic studies

To carry out the necessary measurements, it is important to understand the underlying concepts through which they can be interpreted. Considering firstly the cell system, it is composed of 3 electrodes, a working electrode on whose surface the catalyst is deposited, a counter electrode, and a reference electrode, the system is also filled with a conducting electrolyte.

By inducing a potential difference in the working electrode vs. the counter electrode, the relevant chemical reaction can be observed, as a function of the resulting electrical current. And as a first approach, it can be assumed that the higher the catalytic activity of the material for a given reaction, the higher the resulting current, for the same value of potential difference. This is the basis for voltammetry, by sweeping a given potential range, a graph can be plotted showing current peaks at the potentials at which reactions take place.

In a more in-depth analysis, several factors are analysed to compare different catalysts. Namely, for the OER, onset potential is the potential at which a current density of 1 mA cm^{-2} is achieved. η_{10}, the overpotential at which a current of 10 mA cm^{-2} is reached. j_{400}, the current at an overpotential of 400 mV. And finally, Tafel slope is the value of the potential increase necessary to multiply the current output tenfold.

3. Experimental Procedure

The materials were prepared in collaboration with the Faculty of Chemistry and Faculty of Physical Chemistry, University of Belgrade, Serbia. All of them were synthesised using a procedure similar to the one proposed by Clemente-Juan et al. [13], 22 mM solutions were prepared for five compounds, dissolving $MnSO_4 \cdot H_2O$, $NiSO_4 \cdot 6H_2O$, $(NH_4)_2Fe(SO_4)_2 \cdot 6H_2O$, $CoSO_4$ and $CuSO_4 \cdot 5H_2O$ in 5 mL of deionized water each. Then, 50 mL of a solution of 0.1 M $Na_2WO_4 \cdot 2H_2O$ and 11 mM of Na_2HPO_4 was vigorously stirred with a magnetic

stirrer for 5 minutes. Concentrated acetic acid was then added to this solution to adjust it to a pH of 7. Finally, each solution of transition metal ions was added to 10 mL of tungstate solution, and the obtained mixtures were refluxed for two hours, followed by hot filtering. 0.4 g of KCl was added to the filtrate, and the solutions were left to crystalize overnight. The solutions were then filtered to obtain the crystals, which were then redispersed in deionized water and heated until dissolved. The following day, the recrystallized products were obtained by decanting the excess solution and being left to dry at room temperature. The resulting transition metal POMs were as follows: $K_6Na_4[X_4(H_2O)_2(PW_9O_{34})_2]\cdot 24H_2O$ where X = Ni, Mn, Cu, Co, and Fe respectively for each transition metal POM.

To prepare the composites with different POM to rGO ratios, firstly the amounts of each component, previously ground, were weighed, and 1 mL of ethanol was added. The mixture was then sonicated for 2 h and then left to dry over 2 days. Physico-chemical characterization of materials was done in collaboration with the Faculty of Physical Chemistry, University of Belgrade, Serbia. The synthesized POM/rGO composites were characterized in terms of their structure, present surface functional groups, surface morphology and atomic composition. For the investigation of the structure of the five different POM/rGO materials, an X-ray diffraction (XRD) analysis was performed using a Rigaku Ultima IV diffractometer in Bragg-Brentano geometry, with Ni-filtered CuKα radiation (λ=1.54178 Å). Diffraction data was obtained using scattering angle 2 θ from 20 to 90° with a step of 0.020° and acquisition rate of 2° min^{-1}. Fourier-transform infrared (FTIR) spectroscopy analysis was carried out using Perkin Elmer GX1 spectrometer to determine the surface functional groups of the POMs/rGO samples. Examination of surface morphology and determination of atomic composition was made by Phenom™ ProX Desktop (Thermo Fisher Scientific™, Waltham, MA, USA) scanning electron microscope with integrated energy-dispersive X-ray spectroscopy (SEM-EDX) detector.To discern which of the prepared POM/rGO materials is the best as electrocatalyst for OER and ORR, a single cell was built, with a saturated calomel electrode (SCE) as reference, a platinum coil as counter electrode, and as working electrode a POM/rGO material in the form of a thin film on a glassy carbon rod substrate. All electrodes were placed in 80 mL of 1 M KOH, which was used as the supporting electrolyte. The measurements were done using a Squidstat™ potentiostat from Admiral Instruments.Two sets of studies were done: first set with composites of polyoxometalates coordinated with different transition metals and reduced graphene oxide (rGO), all at a 5:1 ratio of POMs to rGO, and second set for the best POM/rGO with different POM to rGO ratios (1:5, 2:4, 3:3, 4:2, 5:1) as well as with pure rGO and pure POM. Additionally, one sample of 1:5 ratio of POM to activated carbon (AC) was prepared. Catalytic inks were all prepared in the same manner: 6 mg of POM/rGO composites, all at a ratio of 5:1 POM to rGO, were weighted into glass vials, and then 600 µL of deionized water, 400 µL of 96% ethanol, and 25 µL of 0.5 wt.% Nafion™ in ethanol were added. To ensure homogeneity, the inks were all sonicated for 30 minutes in an Emmi® - 08ST sonicator from EMAG Technologies®. To prepare the inks with different POM to rGO ratios, firstly the amounts of each component, previously ground, were weighed, and 1 mL of ethanol was added. The mixture was then sonicated for 2 hours, and finally it was left to dry for 2 days. The inks were then pipetted onto the glassy carbon rod with total area of 0.5 cm^2, leading to a loading of 0.176 mg cm^{-2} of catalyst. Then capacitance measurements were done, all in N_2 saturated solution, achieved by bubbling the electrolyte solution in N_2 for 15 minutes before the experiments and, at a lower flow while running them. After these measurements, O_2 is bubbled in the solution for 5 minutes to remove N_2, at which point OER LSVs were run, 5 for each material. Finally, electrochemical impedance spectroscopy (EIS) was carried out in the frequency range from 100 kHz to 0.1 Hz at several different potentials (1.57, 1.67, and 1.77 V). To study the ORR the samples were tested using cyclic voltammetry with a rotating disk electrode. The same three-electrode electrochemical system was used. 20 µl of ink was applied to the rotating disk electrode. The rotational speed of the disc electrode was varied for each CV, with the rotation speeds being the following: 300, 600, 900, 1200, 1800, 2400, and 3600 rpm. The range of potentials swept was from -0.8 V to 0 V vs. SCE, at a scan rate of 5 mV s^{-1}. iR correction was included during the measurement, performed by a Ivium V01107 Potentiostat/Galvanostat from Ivium Technologies. Finally, a series of experiments were devised to discover which of our POMs is best as a catalyst for metal/air batteries. Firstly, the best metal to use as anode needed to be discovered, so a preliminary cell setup was used, with carbon paper as the current collector on the cathodic side, 1M KOH as electrolyte, and a piece of paper towel as the separator. With this configuration, a few metals were tested, with the selection factor being which had higher open circuit potential. With this criterion, it was determined that the best metal was aluminium plate. With this information combined with other optimization parameters from [12], the final design used was as follows: aluminium plate anode, 4 M KOH electrolyte, cotton pad separator and carbon paper cathodic current collector. With it we tested each POM, with rGO at a ratio of 5:1. The loading of catalytic ink, prepared in the same manner as for the fundamental electrochemical studies, was 800 µL per piece of carbon paper, leading to loadings between 1.73 and 3.55 mg cm^{-2} as is summarised in the next table (Table 1).

Table 1. Loadings of POM/rGO composites on the cathode in a metal-air battery setup.

POM	Loading (mg cm^{-2})
Ni	2.32
Co	3.55
Mn	1.73
Fe	2.32
Cu	2.17

Then, using the metal-air battery setup employing the best POM/rGO as the cathode catalyst, the electrolyte composition was optimised. Thereafter, new power density curves were recorded for batteries with Co-POM/rGO as cathode catalyst, but with KOH electrolyte concentrations of 0.5; 1; 2 and 4 M. At 6M KOH and beyond, the reaction of Al with OH^- became too violent, boiling the electrolyte immediately, causing this attempt, and others at even higher concentrations to be discarded.

4. POM Characterisation

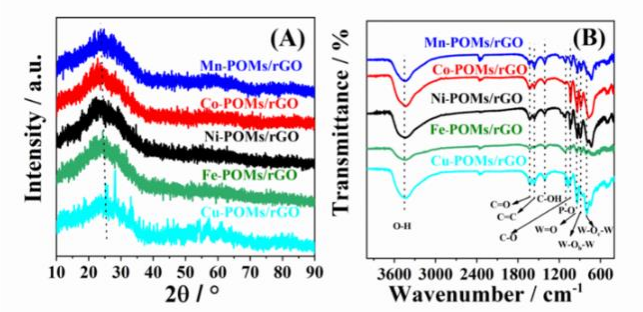

Figure 2. XRD patterns XRD patterns (A), and FTIR spectra (B).

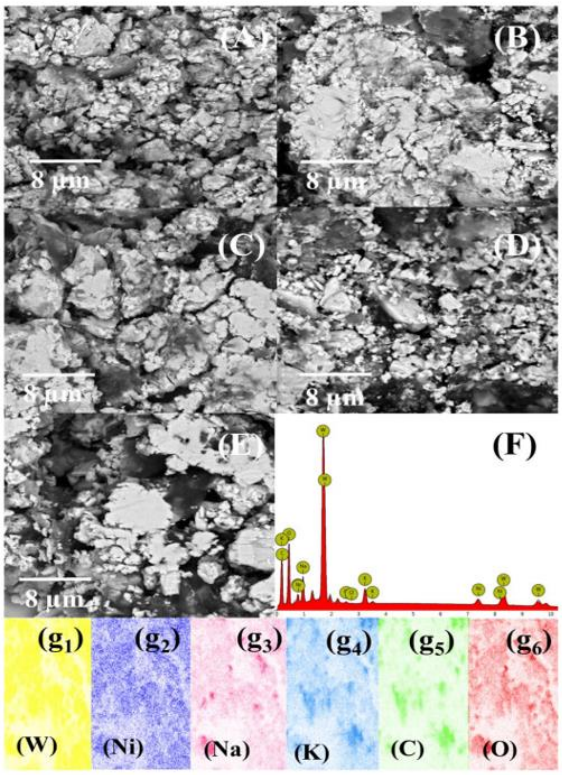

Figure 3. SEM images of Co-POM/rGO(A), Cu-POM/rGO(B), Fe-POM/rGO(C), Mn-POM/rGO(D), and Ni-POM/rGO(E) with EDS spectrum (F) and the elemental mapping of Ni-POMs/rGO(g1-g6).

XRD diffractograms of all studied electrocatalysts are presented in Fig.2(A). All five samples show a broad peak at 2θ of 25° corresponding to the reflections from the rGO crystal planes. Characteristic peaks of POMs structure are not observed because of the highly dispersed state of POMs on the surface of rGO in the synthesized POMs/rGO materials [13-16]. FTIR spectra of POM/rGO composites reveal the four characteristic POMs bands at 1108, 947, 881, and 802 cm^{-1}, Fig.2(B). corresponding to the frequency of P-O in the central PO_4, W=O in the exterior WO_6, W−Ob−W, and W−Oc−W bridges, respectively [15,17-18]. Absorption rGO bands, Fig. 2(B) were observed at 1683, 1561, 1402, and 1038 cm^{-1} and could be associated with C=O, C=C, C-OH, and C-O, respectively [15,19]. The low intensity of rGO bands compared with the intensity of the graphene oxide (GO) absorption band is a consequence of the reduction of oxygen functionalities in rGO [15]. The FTIR spectra of POMs/rGO composite confirmed that the structures of POMs and rGO are preserved in all five samples.

SEM images of the POM/rGO composites, Fig.3(A E), clearly show uniform morphology of all five samples. The typical layered morphology of rGO was observed with POMs nanoparticles anchored to rGO sheets [15-16,19]. The presence of metal (Ni, Co, Mn, Cu, or Fe) within the corresponding POM/rGO composite structure was confirmed by SEM-EDS analysis, Fig.3.(F) illustrates the case of Ni-POM/rGO. Furthermore, elemental mapping revealed uniform distribution of metal in the corresponding composite as well as of elements originating from the POMs/rGO structure (W, Na, K, C, and O), Fig.3. again illustrates the case of Ni- POM/rGO.

5. Determining the best POM for OER

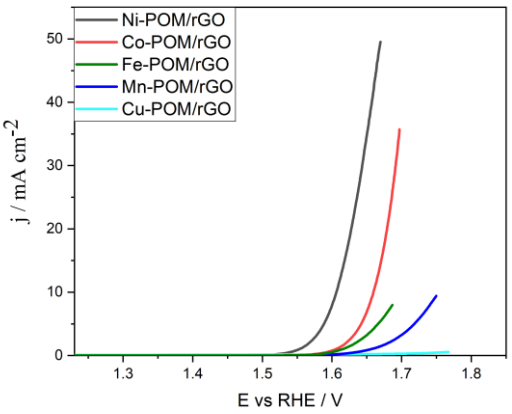

Figure 4. LSVs for different transition metal POM/rGO composites.

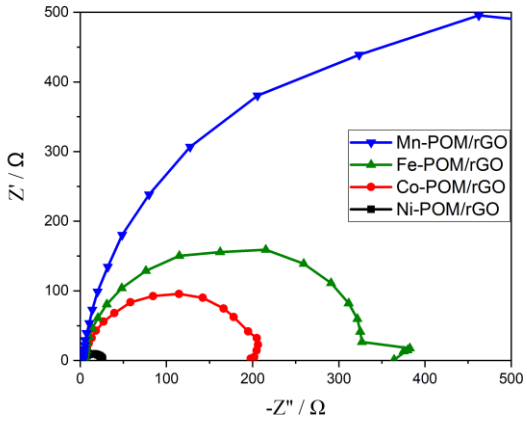

Figure 5. EIS at 1.57V for different POMs.

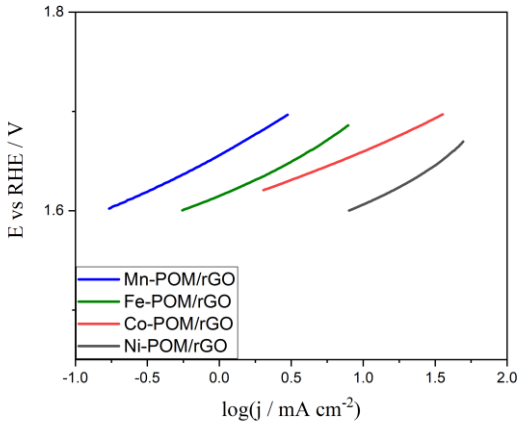

Figure 6. Tafel slopes of different transition metal POM/rGO composites.

For LSV plotting, ohmic drop correction is first made to the measured potentials, accounting for electrolyte resistance. Table 2 summarises the main reaction parameters for OER at studied POM/rGO composites.

Table *2*. Kinetic parameters of OER for POM/rGO (5:1) electrocatalytsts.

Catalyst	Tafel slope (mV dec^{-1})	E_{onset} (V vs RHE)	η_{10} (mV)	j_{400} (mA cm^{-2})
Cu-POM/rGO	naN	naN	naN	0.199
Mn-POM/rGO	66.4	1.656	naN	0.450
Fe-POM/rGO	74.5	1.615	0.467	1.73
Co-POM/rGO	61.8	1.605	0.430	3.07
Ni-POM/rGO	68.1	1.553	0.376	21.8

As the material with the lowest onset potential and j_{400}, it can be determined that Ni-POM is the best, even though its Tafel slope is slightly higher than other studied materials. With this knowledge, we can proceed to the study of which POM to rGO ratio is optimal.

6. Determining the best POM to rGO ratio

After determining that Ni-POM/rGO is the most active for OER, 5 different ratios of POM:rGO were studied, 1:5, 2:4, 3:3, 4:2, 5:1, along with just Ni-POM and just rGO under the same conditions as the studies for different POMs. For comparison, I r O2, a benchmark noble-metal based catalyst was also studied.

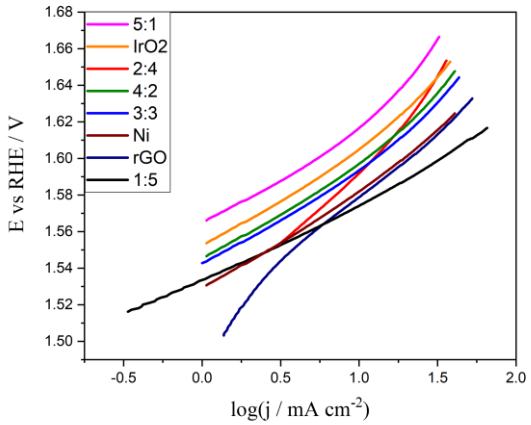

Figure 7. LSVs of Ni-POM/rGO in 1M KOH with different POM:rGO ratios.

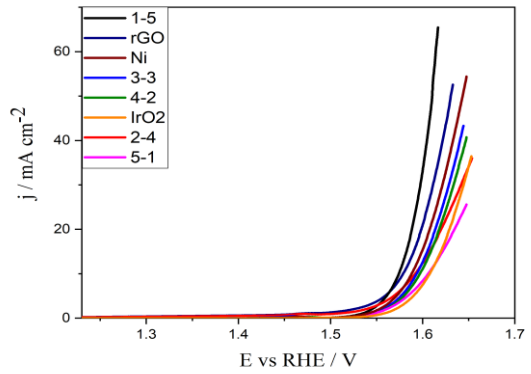

Figure 8. *Tafel slopes of Ni-POM:rGO ratios and IrO2.*

Again, the LSVs immediately reveal the highest current density for a ratio of 1:5 Ni-POM:rGO. E_{onset}, was found to increase in the order rGO (1.46 V) < Ni-POM:rGO (2:4) (1.50 V) < Ni-POM:rGO (1:5) (1.53 V) < Ni-POM:rGO (3:3) (1.54 V) < Ni-POM (1.54 V) < Ni-POM:rGO (5:1) (1.55 V) < Ni-POM:rGO (4:2) (1.55V) < I r O2 (1.56 V).

Furthermore, j_{400} was found to decrease in the order Ni-POM:rGO (1:5) (83.45 mA cm^{-2}) < Ni-POM (53.98 mA cm^{-2}) < rGO (49.43 mA cm^{-2}) < Ni-POM:rGO (3:3) (28.00 mA cm^{-2}) < Ni-POM:rGO (4:2) (27.62 mA cm^{-2}) < Ni-POM:rGO (2:4) (24.19 mA cm^{-2}) < IrO2 (20.61 mA cm^{-2}) < Ni-POM:rGO (5:1) (14.96 mA cm^{-2}). rGO exhibited the lowest overpotential to reach a current density of 10 mA cm^{-2} (η_{10}) of 349 mV, which was just 5 mV and 6 mV lower than that of Ni-POM/rGO (1:5) and Ni-POM, respectively. Next, Tafel analysis was performed,

leading to slopes presented in table 3, where it can be seen that Ni-POM/rGO (1:5) has the lowest slope.

Table 3. Kinetic parameters of OER for Ni-POM/rGO at different ratios and IrO_2.

Catalyst	Tafel slope (mV dec^{-1})	E_{onset} (V vs RHE)	η_{10} (mV)	j_{400} (mA cm^{-2})
Ni-POM:rGO 1:5	42.2	1.53	354	83.45
Ni-POM:rGO 2:4	87.9	1.50	362	24.19
Ni-POM:rGO 3:3	55.3	1.54	364	28.00
Ni-POM:rGO 4:2	55.8	1.55	368	27.62
Ni-POM:rGO 5:1	67.7	1.55	381	14.96
Ni-POM	48.6	1.54	355	53.98
rGO	74.6	1.46	349	49.43
IrO_2	53.4	1.56	378	20.61

Firstly, the lower Tafel slope, Ni-POM/rGO (1:5) is clearly the lowest. The activity of this ratio can also be differentiated from the others by the high value of j_{400}, and low overpotential to reach 10 mA cm^{-2}.

By comparing the values obtained for the studied POMs/rGO with ones from the literature, it can be concluded that our Ni-POM/rGO stacks up very well, having comparable tafel slope to the best material found in other papers [10,11,19].

The study of impedance for these materials follows what is expected, catalysts with higher current density show lower resistance. From all this data it is easy to conclude that of all the POMs studied, and in comparison, with industry benchmark IrO_2, Ni-POM:rGO ratio of (1:5) is the best for OER.

Another observation is that all the materials showed increased activity with each additional LSV run; this may be due to the fact that with each LSV, more nickel oxide is formed, which according to literature [20] has higher activity for OER than metallic Ni, increasing the current with Ni oxide amount.

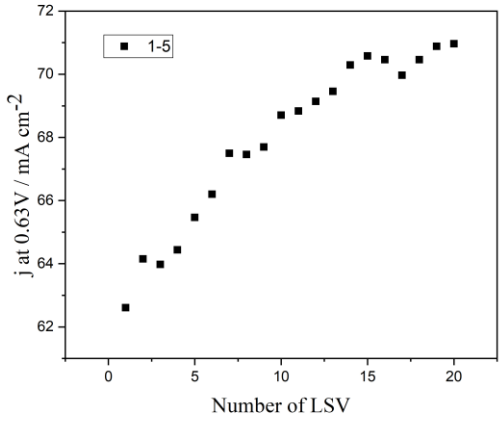

Figure 9. *Current density recorded at 1.63 V using Ni-POM/rGO in 1 M KOH with sequential LSVs.*

But another thing to consider is the catalyst price. By dividing material price per electrode loading, table 4 can be drawn comparing the price of each catalyst per unit of area.

Table 4. Material prices per unit of area.

Catalyst	Cheapest price ($ m^{-2})	Second cheapest price ($ m^{-2})	Sigma Aldrich price ($ m^{-2})
1:5	0.651	2.52	941
2:4	1.04	2.76	753
3:3	1.43	2.99	566
4:2	1.81	3.23	379
5:1	2.20	3.46	192
rGO	0.264	2.29	1128
IrO_2	0.141	0.704	845

The prices were calculated based on three different price points obtained online [21-28].

As we can see, even though Ni-POM has better performance than IrO_2, as the price of rGO is considerably higher than IrO_2, it ends up as more expensive. But, by taking into account performance, another price table can be created.

Table 5. Material prices per unit of current.

Catalyst	Cheapest price (¢ A^{-1})	Second cheapest price (¢ A^{-1})	Sigma Aldrich price (¢ A^{-1})
1:5	0.0780	0.302	113
2:4	0.429	1.14	311
3:3	0.509	1.07	202
4:2	0.656	1.17	137
5:1	1.47	2.31	128
rGO	0.0534	0.463	228
IrO_2	0.0683	0.342	410

By including in the calculations, the current at an overpotential of 400 mV, it can be seen that the Ni-POM/rGO, at a ratio of 1:5 is always cheaper per unit of current produced than its noble metal counterpart. It is also very important to note that both the rGO and POMs studied in this thesis were synthesized in the in the university of Belgrade as a part of a joint project, meaning that both costs are substantially lower than for their commercial counterparts. As the synthesis process is relatively simple and uses cheap sustainable reagents, its scale-up to industrial level would not be a complicated process. From all this it is concluded that, the Ni-POM/rGO studied here outperforms for OER in every way current benchmark IrO_2 electrocatalyst in every way for OER.

7.Study of POM/rGO composites as electrocatalysts for ORR

To investigate potential use of POM/rGO composites as bifunctional electrocatalysts for oxygen electrode in metal-air batteries, i.e., for both OER and ORR, performance of POM/rGO composites was evaluated under ORR polarization conditions. ORR study was done using Ni-POM/rGO (1:5) and CoPOM/RGO (1:5) as the best and second-best electrocatalysts for OER among the five tested composites. To confirm materials' activity for ORR, two CVs are recorded for each material, in N_2- and O_2-saturated solution, (Figure 10 and 11). Comparison of the recorded current densities shows clear increase in the presence of O_2 in case of both composites originating in the reduction of oxygen. Furthermore, it is evident that Co-POM/rGO (1:5) exhibits higher performance under ORR polarization conditions than Ni-POM/rGO (1:5) with current densities recorded using Co-POM/rGO being double those recorded using Ni-POM/rGO.

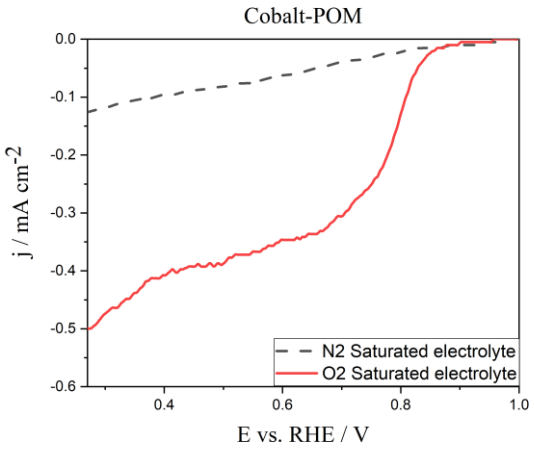

Figure 10. *Cathodic scan of CVs of Co-POM/rGO (1:5) in N_2- and O_2-saturated 1 M KOH.*

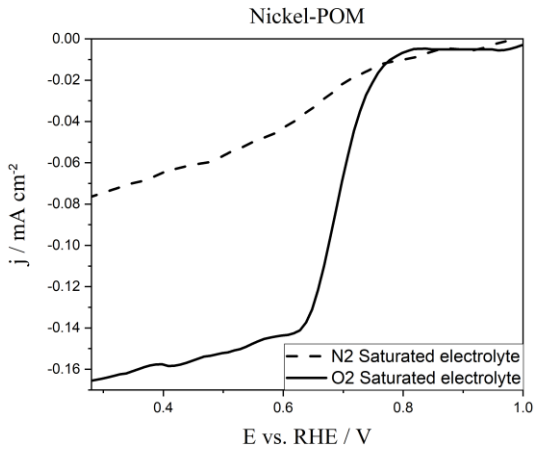

Figure 11. *Cathodic scan of CVs of Ni-POM/rGO (1:5) in N_2- and O_2-saturated 1 M KOH.*

Subsequently, CVs were recorded using different electrode rotation rates, Figure 12. Onset potential (E_{onset}) as a measure of the electrocatalyst's activity, can be determined using different approaches in case of ORR. E_{onset} can be determined as the potential at which the recorded current density clearly deviates from the background current density. It can also be determined as the intersection point of the tangents to the baseline and to the rising current density part of CV. Finally, E_{onset}, can be defined as potential at the current density of -3 µA cm^{-2}. The onset potentials of two investigated electrocatalysts were determined (from CV curves at 1600 rpm) to be 0.767 and 0.719 V for Co-POM and Ni-POM respectively. Thus, Co-POM/rGO (1:5) showed more positive onset potential compared to Ni-POM/rGO (1:5) indicating its higher activity for ORR. Additionally, half-wave potential ($E_{1/2}$), as another widely-used indicator for the evaluation of the electrocatalytic activity of new electrode materials, was found to have a more positive value for Co-POM/rGO (1:5) (0.677 V) compared to Ni-POM/rGO (1:5) (0.620 V). Koutecký-Levich analysis was next performed at 3 different potentials in order to determine the number of electrons (n) transferred during ORR (j^{-1} vs. $w^{-1/2}$), Figure 13. ORR n values for Co-POM/rGO (1:5) were found to range from 2.6 to 2.7 suggesting that reduction of oxygen proceeds by both 2-electron pathway (with production of $(HO_2)^-$ as an intermediate) and 4-electron pathway (O_2 directly reduced to OH^-). 4-electron pathway is favourable mechanism for ORR in electrochemical energy conversion devices. On the other hand, n value for Ni-POM/rGO (1:5) was evaluated to range from 1.7 to 1.8 indicating a two-electron mechanism.

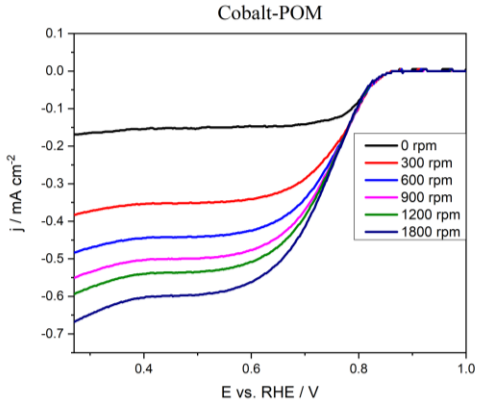

Figure 12. *LSVs for Co-POM/rGO at different electrode rotation rates.*

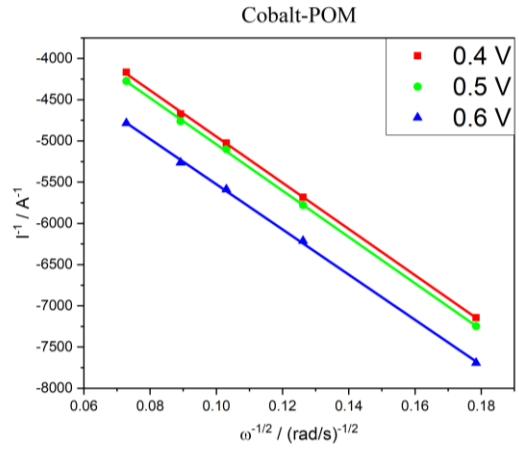

Figure 13. *Koutecký-Levich analysis of Co-POM at three different potentials*

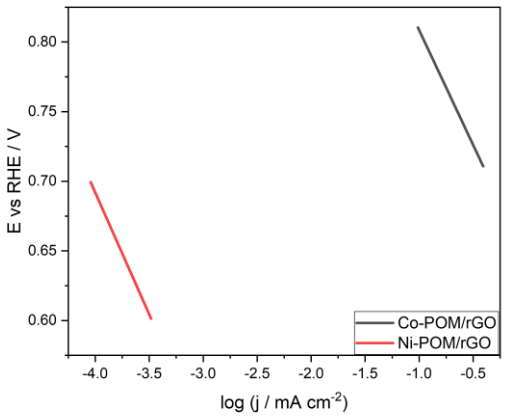

Figure 14. *Tafel plots of the Co-POM/rGO (1:5) and Ni-POM/rGO (1:5) for ORR*

More positive onset and half-wave potentials, lower Tafel slope and higher number of electrons exchanged clearly demonstrate superior performance of Co-POM/rGO for ORR compared to Ni-POM/rGO.

8.Metal-Air Batteries

The last set of experiments carried out were the construction and study of metal-air batteries.

Firstly, the optimum metal to use as anode needed to be determined, so a preliminary cell setup was used, with carbon paper as the current collector on the cathodic side, 1 M KOH as the electrolyte, and a piece of paper towel as a separator. With this configuration, a few metals were tested, with the selection factor being the cell's open circuit potential. And aluminum was found to be the optimum one.

Using the set-up already described, with Al plate, cotton separator, KOH electrolyte and catalyst deposited on carbon paper, firstly, the OCPs of all POMs were obtained with the use of a UNI-T 0T70B multi-metre, and they were, in ascending order, Ni-POM/rGO (1.386 V) < Co-POM/rGO (1.395 V) < Fe-POM/rGO (1.396 V) < Mn-POM/rGO (1.448 V) < Cu-POM/rGO (1.529 V). Then, all the materials were studied for the discharge of the battery leading to the following power density curves.

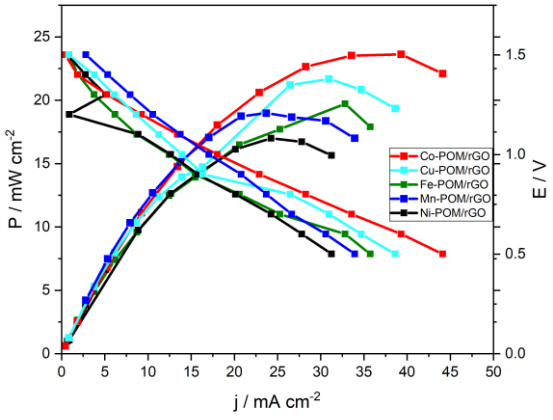

Figure 15. *Power density curves of MAB with different POM/rGO composites as cathode electrocatalyst.*

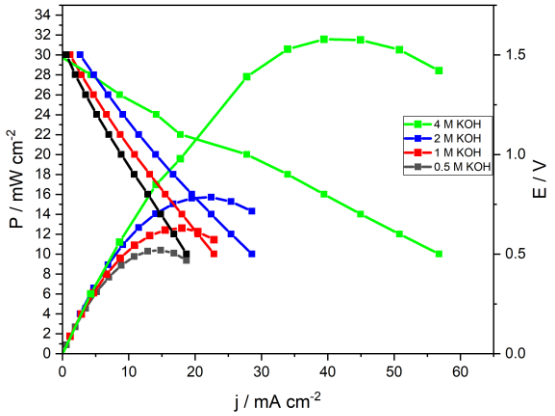

Figure 16. *Power density curves of MAB with different POM/rGO composites as cathode electrocatalyst.*

The maximum power densities obtained were, in ascending order, Ni-POM/rGO (17.0 mW cm^{-2}) < Mn-POM/rGO (19.0 mW cm^{-2}) < Fe-POM/rGO (19.7 mW cm^{-2}) < Cu-POM/rGO (21.7 mW cm^{-2}) < Co-POM/rGO (23.6 mW cm^{-2}).

As can be seen, and as was expected, Co-POM/rGO has the highest energy density value. This is expected because the main reaction involved in metal-air battery discharge is ORR for which Co-POM/rGO was the best material.

One final study was carried out in the metal-air batteries, for the best material, several electrolyte concentrations were studied to enhance battery performance. As a final result, it can be observed that 4 M KOH was indeed the concentration for which the best results were reached.

8. Conclusions

POMs are a unique class of materials that have been shown to be suitable for improving performance on a variety of processes, following different approaches, from the very simple addition of POMs to activated carbon paste electrodes to more complex methods of chemical linking to emerging nanomaterials. As discussed, using POMs in batteries and supercapacitors (SCs) can enhance energy density by efficiently contributing to pseudocapacitive charge storage effects from their high surface-to-bulk ratio and multiple redox states. POMs are cheaper and easier to obtain in larger quantities than the noble metals based electrocatalysts which are currently the most active ones for the mentioned devices. Hence, their application holds the promise of contributing to overcoming the challenges of upgrading modern energy systems into more sustainable ones.

It is critical to develop new POM-based composites, particularly because of their poor electrical conductivity and high solubility in battery electrolytes, which results in low cycling stability and

poor rate performance. Linking POMs to an appropriate conducting scaffold remains thus both fundamental and problematic. Particular attention should be given to POMs when used as electrode materials linked to carbon nanostructures that can potentially increase the conductivity of POMs. The energy storage mechanism for POMs-based electrode materials for rechargeable batteries and SCs is still not fully understood; the higher number of electron exchanges per molecule, when compared to other redox materials used in battery storage, makes it more complex to grasp. In the future, more in depth analysis will be necessary to understand the reactions at the electrode/electrolyte interface.

In this study, XRD, FTIR, and SEM-EDS techniques were used for the analysis of the structure and morphology of five different POMs/rGO electrocatalysts. SEM-EDS results showed the presence of five different metals (Ni, Co, Mn, Cu, and Fe) inside the POMs/rGO samples. FTIR spectra of NiPOMs/rGO, Co-POMs/rGO, Mn-POMs/rGO, Fe-POMs/rGO, and Cu-POMs/rGO electrocatalysts displayed characteristic bands for POMs and rGO structures.

And with the study of the conjugations of POMs and carbon structures, we could see that rGO addition significantly increased the currents for all reactions. For OER, Ni-POM/rGO was clearly the superior candidate, and further studies showed that the optimal Ni-POM:rGO ratio was 1:5. The current density values obtained with this catalyst were very promising, being even higher than that of IrO_2, the catalyst currently considered the best for this reaction. It is also important to note that even though Co-POM/rGO was not as good as Ni-POM, it came second best for OER.

In terms of ORR, Co-POM/rGO was the best; this, conjugated with the results from the MAB testing, lead us to conclude that Co-POM/rGO has very interesting as a bifunctional electrocatalyst for rechargeable metal-air batteries.

Even though more in-depth studies of metal-air battery construction were not covered in the scope of this project, it would be interesting to analyse the results with the change of different parameters, namely separator composition, metal plate used, and even different carbon supports for the catalyst.

References

[1] url: https://gadebate.un.org/en/77/secretary-general-united-nations (visited on 01/10/2022).

[2] U. Ghosh et al. “Review – Hydrocracking using different catalysts”. In: Chem. Process Eng. Res. 34 (2015), pp. 51–56.

[3] H. Wang et al. “Molecular cluster batteries of nano-hybrid materials between Keggin POMs and SWNTs”. In: Dalt. Trans. 41 (2012), pp. 9863–9866. doi: 10.1039/c2dt30603d.

[4] H. Wang et al. “In operando X-ray absorption fine structure studies of polyoxometalate molecular cluster batteries: Polyoxometalates as electron sponges”. In: J. Am. Chem. Soc. 134 (2012), pp. 4918–4924. doi: 10.1021/ja2117206.

[5] J. Chen et al. “Metal hydride mediated water splitting: Electrical energy saving and decoupled H2/O2 generation”. In: Mater.Today 47 (2021), pp. 16–24. doi: 10.1016/j.mattod.2021.02.019.

[6] S.A. Grigoriev et al. “Current status, research trends, and challenges in water electrolysis science and technology”. In: Int. J. Hydrogen Energy 45 (2020), pp. 26036–26058. doi: 10.1016/j.mattod.2021.02.019.

[7] N. Kawasaki et al. “Nanohybridization of polyoxometalate clusters and single-wall carbon nanotubes: Applications in molecular cluster batteries”. In: Angew. Chemie - Int. Ed. 50 (2011), pp. 3471–3474. doi: 10.1002/anie.201007264.

[8] X. López, J.A. Fernández, and J.M. Poblet. “Redox properties of polyoxometalates: New insights on the anion charge effect”. In: J. Chem. Soc. Dalt. Trans. 6 (2005), pp. 1162–1167. doi: 10.1039/b507599h.

[9] X. López, C. Bo, and J.M. Poblet. “Electronic properties of polyoxometalates: Electron and proton affinity of mixed-addenda Keggin and wells-dawson anions.” In: J. Am. Chem. Soc. 124 (2002), pp. 12574–12582. doi: 10.1021/ja020407z.

[10] N. Limani et al. “Cobalt Phosphotungstate-based composites as bifunctional electrocatalysts for oxygen reactions”. In: Catalysts 12 (2022). doi:10.3390/catal12040357.

[11] C. Singh and S.K. Mukhopadhyay S.and Das. “Polyoxometalate-supported Bis(2,2-bipyridine) mono(aqua)nickel(II) coordination complex: An efficient electrocatalyst for water oxidation”. In: Inorg. Chem. 57 (2018), pp. 6479–6490. doi:10.1021/acs.inorgchem.8b00541.

[12] F. Pan and Q. Wang. “Redox species of redox flow batteries: A review”. In: Molecules 20 (2015), pp. 20499–20517. doi: 10.3390/molecules201119711.43

[13] J. M. Clemente-Juan et al. “Increasing The Nuclearity of Magnetic Polyoxometalates. Syntheses, Structures, and Magnetic Properties of Salts of the Heteropoly Complexes $[Ni_3(H_2O)_3(PW_{10}O_{39})H_2O]^{7-}$, $[Ni_4(H_2O)_2(PW_9O_{34})_2]^{10-}$, and $[Ni_9(OH)_3(H_2O)_6(HPO_4)_2(PW_9O_{34})_3]^{16-}$”. In: Inorg. Chem.1.38(1999), pp. 55–63. doi: https://doi.org/10.1021/ic9807902.

[14] A. Ucar et al. “Catalytic degradation of organicdye using reduced graphene oxide polyoxometalate nanocomposite”. In: Materials Chemistry and Physics 196 (2017), pp. 21–28. doi: 10.1016/j.matchemphys.2017.04.047.

[15] F. Dehghani Sanij et al. “Fabrication of polyoxometalate-modified palladium-nickel/reduced graphene oxide alloy catalysts fo renhanced oxygen reduction reaction activity”. In: RSC Advances 11

(2021), pp. 39118–39129. doi: 10.1039/d1ra06936e.
[16] N. Ross and N. Civilized Nqakala. “Electrochemical Determination of Hydrogen Peroxide by a Non enzymatic Catalytically Enhanced Silver-Iron(III) Oxide/Polyoxometalate/ReducedGraphene Oxide Modified Glassy Carbon Electrode”. In: Analytical Letters 53 (2020), pp. 2445–2464. doi:10.1080/00032719.2020.1745223.44
[17] A. Khodadadi Dizaji, H.R. Mortaheb, and B. Mokhtarani. “Preparation of supported catalyst byad-sorption of polyoxometalate on graphene oxide/reduced graphene oxide”. In: Materials Chemistry and Physics 199 (2017), pp. 424–434. doi:10.1016/j.matchemphys.2017.07.016.
[18] A. Tarlani et al. “Immobilization of Keggin and Preyssler tungsten heteropolyacids on various functionalized silica”. In: Journal of Colloid and Interface Science 303 (2006), pp. 32–38. doi: 10.1016/j.jcis.2006.07.024.
[19] M.L. Yola et al. “Sensitive and selective determination of aqueous triclosan based on gold nanoparticles on polyoxometalate/reduced graphene oxide nanohybrid”. In: RSC Advances 5 (2015), pp. 65953–65962. doi: 10.1039/c5ra07443f.
[20] Matthias Steimecke et al. “Higher Valent Nickel Oxides with Improved Oxygen Evolution Activity and Stability in Alkaline Media Prepared by High-Temperature Treatment of Ni(OH) 2”. In: ACS Catalysis (Feb. 2020). doi:10.1021/acscatal.9b04788.
[21] url: https://www.alibaba.com/product-detail/99 - 99-Top-Quality-reduced-graphene_1600233768465.html?spm=a2700.7724857.normal_offer.d_title.166661cdt90BF5 (visited on 01/09/2022).
[22] url: https://www.alibaba.com/product-detail/Reduced-Graphene-Oxide-Graphene-Oxide-Price_62409775857.html?spm=a2700.galleryofferlist.normal_offer.d_title.257b69cfnj4Her&s=p (visited on 01/09/2022).
[23] url: https://www.sigmaaldrich.com/PT/en/product/aldrich/805424 (visited on 01/09/2022).
[24] url: https : / / www . alibaba . com / product - detail / IrO2 - Nanoparticles - Iridium - dioxide - Iridium-Oxide_1600262487085.html?spm=a2700.7724857.normal_offer.d_title.54101b16la2nov (visited on 01/09/2022).
[25] url: https://www.alibaba.com/product-detail/Iridium-Oxide-Factory-Price-Sell-Nano_62424384729.html?spm=a2700.7724857.normal_offer.d_title.54101b16la2nov&s=p (visited on 01/09/2022).
[26] url: https://www.sigmaaldrich.com/PT/en/product/aldrich/206237 (visited on 01/09/2022).
[27] url: https://www.sigmaaldrich.com/PT/en/product/sigma/t2786?gclid=Cj0KCQjwhqaVBhCxARIsAHK1tiMMzjS9p23HJNLtL43WcnVADTo-4XuO-JAf7HloecaAqNAEALw_wcB (visited on 01/09/2022).
[28] url: https://www.sigmaaldrich.com/PT/en/product/sial/p4006 (visited on 01/09/2022).